Invited Paper to
Particle Accelerator Conference 2001
Chicago, IL, June 18-22, 2001

BNL-67992

RF system for the SNS Accumulator ring*

M. Blaskiewicz†,
J.M. Brennan, J. Brodowski, J. Delong, M. Meth, K. Smith, A. Zaltsman
BNL, Upton NY 11973, USA

Abstract

During accumulation the RF beam current in the the spallation neutron source ring rises from 0 to 50 amperes. A clean, 250 nanosecond gap is needed for the extraction kicker risetime. Large momentum spread and small peak current are needed to prevent instabilities and stopband related losses. A robust RF system meeting these requirements has been designed.

1 INTRODUCTION

In broad terms, the Spallation Neutron Source consists of a linear accelerator, accumulator ring, and mercury target[1, 2]. The linear accelerator produces a 1 GeV, H^- beam which is charge exchange injected for $\approx$ 1000 turns. After accumulation the beam is extracted using a fast kicker and sent to the mercury target. The purpose of the accumulator ring RF system is to maintain a gap for the rise time of the extraction kicker while maintaining low peak beam current and large momentum spread[3, 4, 5]. The latter considerations prevent space charge stopband related losses and coherent instabilities. Table 1 summarizes RF related machine parameters.

* Work performed under the auspices of the United States Department of Energy

† blaskiewicz@bnl.gov

parameter	value
circumference	248m
transition gamma	5.25
total h=1 voltage	40 kV
h=1 gap capacitance	3 nF
total h=2 voltage	20 kV
h=2 gap capacitance	0.75 nF
space charge Z/n	i200 Ω
proton kinetic energy	1 GeV
injected bunch length	610 ns
injected energy spread	±3.8MeV, full
protons at extraction time	2.08×10^{14}
accumulation time	1100 turns
extraction gap	250ns
repetition rate	60 Hz

Table 1: Machine Parameters

2 CAVITY AND POWER AMPLIFIER

Harmonic numbers of 1 and 2 imply RF frequencies of $f_1 = 1.05$ MHz and $f_2 = 2.11$ MHz. Each cavity is composed of two RF gaps driven in parallel by the power amplifier. The $h = 1$ cavities are designed for a gap voltage of $V_g = 10$ kV and the $h = 2$ cavities are identical but for less gap capacitance. Inductance is supplied by coaxial stacks of Phillips 4M2 ferrite. There are 21 rings per gap and each ring is 2.72cm thick. The rings have inner and outer diameters of 25 cm and 50 cm, respectively.

A large magnetic field in the ferrite cuts down on the total cavity length. The AGS Booster uses the same ferrite, the same 2 to 1 ratio of outer to inner radius, and similar frequency range. Assuming the same RF magnetic field an $h = 1$ gap field of 13kV can be supported without Q losses or similar ferrite problems. Assuming the magnetic field varies as $1/r$ within the ferrite, the magnetic field has a maximum RF amplitude of $B_{rf} = 31$ mT for $V_g = 10$ kV. The cavity resonant frequency is tuned using bias current which flows in opposite directions through the two cells leading to negligible RF voltage across the bias supply. The baseline design calls for a constant resonant frequency during the cycle, but the possibility of dynamically tuning the cavity is a principle area of R&D. The first article cavity has been built. Low power measurements of the resonant frequency and R/Q, with no bias, agreed with design values at the few percent level.

The design of the power amplifier is driven by beam loading requirements. During the millisecond of accumulation the average beam current rises from 0 to 34 A. The maximum amplitude of the first harmonic component is $I_1 = 50$ A and the second harmonic component is down by a factor of 10. The philosophy here is to design the power amplifier for $h = 1$ and use the same design for $h = 2$. This reduces EDIA significantly and allows the $h = 2$ system to to be easily modified to $h = 1$ if desired. The base line design requires the power amplifier to fully compensate the beam current while providing the necessary quadrature component to drive the gap voltage. The cavity resonant frequency is fixed, and equal to the RF frequency. In some sense this may be pessimistic but the consequences of this assumption to the overall system cost are not great, whereas the benefits for system performance and reliability are very valuable.

A Thompson (TH558) tetrode drives two gaps in parallel while supplying the necessary anode current. With three cavities (6 accelerating gaps) at $h = 1$ and 7 kV/gap the anode dissipation reaches 500 kW at the end of accumula-

tion. The time average dissipation is much smaller, about 50 kW, but very high reliability is required and stressing the tube could lead to shorter life. The $h = 2$ system has one cavity with two gaps and 10 kV/gap. The $h = 2$ beam loading is much smaller than for $h = 1$.

Since the RF system is on for ~ 2 ms every 16.7 ms, the tube will be biased off for most of the time. The grid bias supply can switch between cutoff and quiessant states in $\approx 100\mu$s. An anode power supply consists of two, charging 14 kV, 3 A supplies and capacitor bank. The total capacitance of the bank is 75μF. For a 10 A draw starting at 10 kV, with a charging current of 6 A the anode voltage droops by 3% over 2 ms.

Every effort is being made to reduce surprises during commissioning. Toward this end a full power beam-cavity simulator is planned. This device would use one power amplifier to drive the cavity, and another to simulate the beam. The beam circuit will be attached to the anode of the beam PA and encircle the ferrite stack of the cavity. The low level drive for the simulator will mimick both dipole and quadrupole beam oscillations. In this way we will test the tuning scheme, the high level RF system, and the low level RF system well before installation.

3 VOLTAGE CONTROL AND BEAM STABILITY

In analytic models of steady state beam loading [6, 7, 8] the ratio of beam induced voltage to total gap voltage plays an important role. For SNS this beam loading parameter is ~ 3, so the stability if the RF system could be compromised. Unlike typical accelerators, the SNS cycle time is comparble to the synchrotron period, so the transient response of the beam-cavity interaction is very important. Additionally, the dual harmonic system leads to very nonlinear dynamics and analytic results are difficult to obtain. Therefore, simulations of the beam-cavity system have been a primary design tool.

A schematic of the beam, cavity and generator for a single gap cavity is shown in Figure 1. The electric field in the gap, E_g is related to the gap voltage V_g and the equivalent gap length ℓ_g via $E_g\ell_g = -V_g$. The beam current, I_b is positive to the left so a positive value of V_g accelerates the beam. Suppose the system is quiessant for $t < 0$. The anode current I_A, gap voltage and beam current are related via

$$\frac{I_A(t) - I_A(0)}{n_{gap}} - I_b(t) = \frac{V_g(t)}{R_f} + C_g\frac{dV_g(t)}{dt} + \frac{1}{L_g}\int_0^t V_g(t')dt', \quad (1)$$

where C_g and L_g are the equivalent capacitance and inductance of one gap, R_f is the shunt impedance of the ferrite for one gap, and $n_{gap} = 2$ is the number of gaps driven by one power amplifier. The anode voltage V_A, gap voltage, and anode supply voltage B^+ are related via $V_A(t) + V_g(t) = B^+$. With only a few percent droop, the anode supply voltage was assumed constant. The final relation involves the anode current, grid drive voltage V_G and anode voltage. For reasonable parameters the anode voltage depends only on the combination $V_A + \mu V_G$ where the amplification factor μ depends only on the screen voltage, which is held constant during the cycle. Figure 2 shows $I_A = G(V_A + \mu V_G)$ for the TH558 tetrode with a screen voltage of 2 kV.

The RF control loops directly affect the grid drive voltage so in equation (1) set

$$I_A(t) = G(B^+ - V_g(t) + \mu V_G(t)).$$

The grid drive voltage is taken to be

$$V_G(t) = I_G(t)\sin(\omega_{rf}t) - Q_G(t)\cos(\omega_{rf}t) + \bar{V}_G,$$

where ω_{rf} is the ideal RF frequency, $\bar{V}_G$ is a DC offset and the in phase I_G and quadrature Q_G amplitudes vary slowly. The ideal RF frequency is set before injection begins and the phase is chosen so that extraction can be defined to better than one turn.

Since the beam current is not a pure sinusoid, the gap voltage is not a pure sinusoid. However, the in phase I_g and quadrature Q_g components of the gap voltage at ω_{rf} can be defined with respect to a given measurement procedure. The control system will be digital, so a natural unit of time is one turn. Define the raw in phase and quadrature components of the gap voltage on the nth turn to be

$$I_g^0(n) = \frac{2}{T_{rf}}\int_{(n-1)T_{rf}}^{nT_{rf}} \sin(\omega_{rf}t)V_g(t)dt, \quad (2)$$

$$Q_g^0(n) = -\frac{2}{T_{rf}}\int_{(n-1)T_{rf}}^{nT_{rf}} \cos(\omega_{rf}t)V_g(t)dt. \quad (3)$$

In the actual system these might be generated by digital FIR filters but for any reasonable clock rate there will be little difference between the analog and digital quantities. The raw values are then subject to delay and smoothing to create the inputs to the control system. This is modeled as a lagged, auto-regressive filter,

$$I_g(n+1) = \delta I_g(n) + (1-\delta)I_g^0(n - n_g), \quad (4)$$

$$Q_g(n+1) = \delta Q_g(n) + (1-\delta)Q_g^0(n - n_g), \quad (5)$$

where $\delta = \exp(-T_{rf}r_g)$, r_g is the accumulation rate, and n_g is the signal delay in turns. The lower limit on the delay is set by the round trip time between the ring and the RF control room, $n_gT_{rf} \gtrsim 750$ ns.

In general the in phase and quadrature components of the gap voltage will not be equal to their target values $\hat{I}_g(n)$ and $\hat{Q}_g(n)$. The first level of RF control varies the grid drive amplitudes I_G and Q_G to approach the desired values of the gap voltage components I_g and Q_g. To obtain

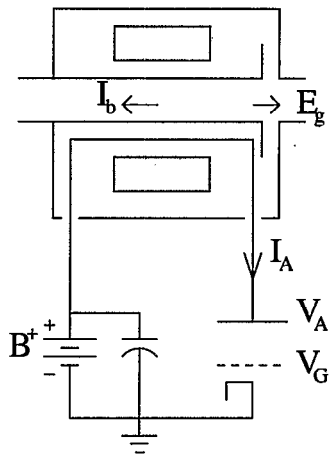

Figure 1: Equivalent beam-cavity circuit.

the feedback matrix assume that the error is small and define the error terms $\Delta I_G, \Delta I_g, \Delta Q_G, \Delta Q_g$. Inserting these errors in equation (1) and keeping first order terms yields

$$\begin{pmatrix} \Delta I_G \\ \Delta Q_G \end{pmatrix} = \frac{n_{gap} R_A}{\mu |Z_\ell|} \begin{pmatrix} \cos\phi_z & -\sin\phi_z \\ \sin\phi_z & \cos\phi_z \end{pmatrix} \begin{pmatrix} \Delta I_g \\ \Delta Q_g \end{pmatrix} \tag{6}$$

where R_A is the anode resistance and Z_ℓ is the loaded impedance of the cavity. The detuning angle is given by

$$\tan\phi_z = \frac{R_\ell}{\omega_{rf} L_g} - \omega_{rf} C_g R_\ell, \tag{7}$$

where R_ℓ is the loaded shunt impedance of the gap. For feedback loops define a low level gain G_g. The low level loops cause the grid drive signal to change according to

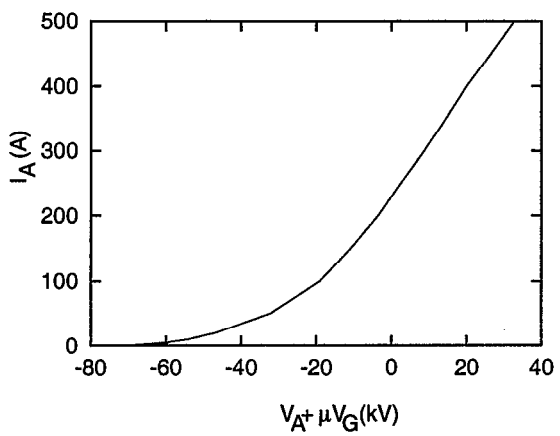

Figure 2: Anode current versus effective voltage for a screen voltage of 2 kV. The amplification factor is $\mu = 132$

$$\frac{d}{dn}\begin{pmatrix} I_G \\ Q_G \end{pmatrix} = G_g \begin{pmatrix} \cos\phi_z & -\sin\phi_z \\ \sin\phi_z & \cos\phi_z \end{pmatrix} \begin{pmatrix} \hat{I}_g - I_g \\ \hat{Q}_g - Q_g \end{pmatrix}. \tag{8}$$

The detuning angle is zero in the baseline design but, anticipating dynamic tuning, take it to be given by equation (7) with R_ℓ replaced by a constant. Assuming that $L_g(n)$ and and C_g are reasonably well known, all the parameters of the voltage feedback loop are defined.

Along with the voltage feedback the design calls for a feed-forward correction using the measured beam current. Assume the in phase I_B and quadrature Q_B components of the beam current are measured using the same algorithm as for the in phase and quadrature components of the gap voltage. Let r_B and n_B be the accumulation rate and delay for the acquisition of the beam current components. The feed forward correction for the beam current is taken to be

$$\begin{pmatrix} I_G^1 \\ Q_G^1 \end{pmatrix} = G_f \frac{n_{gap} R_A}{\mu} \begin{pmatrix} I_B - \hat{I}_B \\ Q_B - \hat{Q}_B \end{pmatrix}, \tag{9}$$

where $\hat{I}_B$ and $\hat{Q}_B$ are the in phase and quadrature components of beam current for which the cavity is tuned. For an accurate value of R_A the ideal feed forward gain is $G_f = 1$. Let I_G^2 and V_G^2 be the solutions to equation (8) then, with the feed forward correction given by equation (9) the high frequency grid drive signal is given by

$$\begin{aligned} V_G(t) = &(I_G^1 + I_G^2 + I_G^0)\sin(\omega_{rf} t) \\ &- (Q_G^1 + Q_G^2 + Q_G^0)\cos(\omega_{rf} t) + \bar{V}_G, \end{aligned} \tag{10}$$

where I_G^0 and Q_G^0 are best guess values for the amplitude functions which are based on the behavior during earlier cycles. The in phase and quadrature amplitudes are defined at the beginning of each turn and linearly interpolated between turns.

The RF simulation uses standard techniques[9]. The previous equations are transformed into a set of first order differential equations and discretized. The total RF kick is updated once per particle per turn with 360 time slices per turn. Space charge makes a significant contribution to the longitudinal force. For frequencies below $f_{rf}^2/4\pi h f_s \sim 75$ MHz the space charge forces can be updated once per turn. At the reference azimuth the voltage due to space charge is

$$V_{sc}(t) = \frac{Z_{sc}}{\omega_0} \frac{dI_b(t)}{dt}, \tag{11}$$

where $Z_{sc} \approx 200\Omega$ is the space charge impedance[10]. The space charge kick was obtained by convolving the binned beam current with a differentiated, 50ns pulse. The beam is modeled by $M \sim 10^4$ macro-particles. The beam current on nth turn is a sum over macro-particles and a binning/smoothing function $f(t)$ is used to reduce unphysical high harmonics

$$I_b(t) = \sum_{k=1}^{M} f(t - t_n^k).$$

The change in proton energy depends on arrival time at the gap.

$$E^k_{n+1} = E^k_n + qV_{total}(t^k_n),$$

where the total voltage is $n_{cav}n_{gap}V_{gap}$ plus 2nd harmonic and space charge. Arrival time on the next turn changes depending on the energy deviation

$$t^k_{n+1} = t^k_n + \eta T_{rev}\frac{E^k_{n+1} - E_0}{E_0\beta^2}.$$

Table 1 summarizes the RF parameters. Notice that the injected energy spread is ±3.8MeV with a rectangular distribution. This is created by an energy wiggler cavity running at a slightly different frequency from the LINAC RF. The net effect is to broaden the rms width of the energy distribution without creating the tails associated with a debuncher cavity. The simulations assumed 2 turns of delay and the accumulation rates r_g and r_B were taken to be $100/ms$. The target $h = 1$ RF voltage was ramped from 30 to 40 kV over the first 500 turns. To be pessimistic, the best guess values of the in phase and quadrature grid drive voltages were nulled $I^0_G = Q^0_G \equiv 0$. Only the voltage error and feed forward signals, via equations (8) and (9), created the grid drive voltage for $h = 1$. With its smaller beam loading, the $h = 2$ voltage was set to half the $h = 1$ target value throughout the cycle.

Figure 3 shows the longitudinal phase space, the rf bucket, and the edges of the kicker gap just before extraction. Figure 4 shows the bunch current, the space charge voltage and the total RF voltage just before extraction. The gap is clean and the bunching factor is 0.4.

The phase and amplitude loops are necessary, but the RF system is fairly robust with respect to feed forward errors. Figure 5 illustrates the situation when there is no feed forward. The maximum error in the RF voltage waveform is $\lesssim$5 kV and the bunch is acceptable. However, with the heavy beam loading, feedforward is required for system stability and a small, unstable, oscillation exists without it. In practice, even with marginal feed forward the RF system should easily meet its specifications.

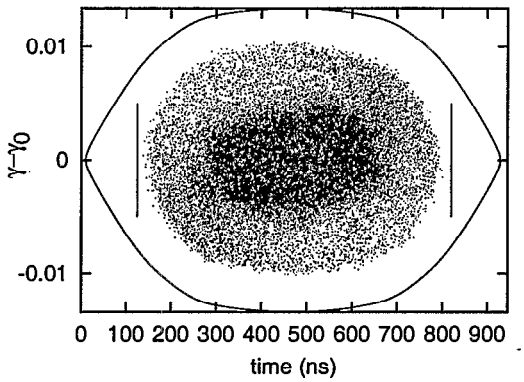

Figure 3: Phase space distribution and bucket at extraction for nominal design.

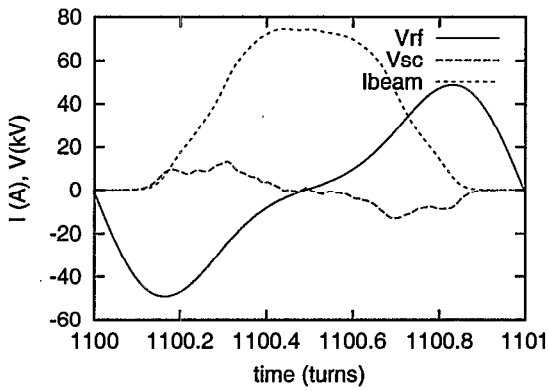

Figure 4: Currents and voltages at extraction for nominal design. The binned current, convolved with a 50ns smoothing pulse, is shown.

4 DYNAMIC TUNING

By changing the cavity resonant frequency as the beam is stacked the amount of RF drive current can be reduced. Conversely, the $h = 1$ gap voltage can be increased. For a steady state system with beam current $I_b(t) = \hat{I}_b\cos(\omega_{rf}t)$ and gap voltage $V_g(t) = \hat{V}_g\sin(\omega_{rf}t)$, the minumum RF anode current is $I_A(t) = (n_{gap}\hat{V}_g/R_f)\sin(\omega_{rf}t)$ and the cavity resonant frequency is

$$\omega_{res} = \omega_{rf}\left(1 + \frac{\hat{I}_b}{\hat{V}_g C_g \omega_{rf}}\right)^{1/2}. \qquad (12)$$

Since $\omega_{res} = 1/\sqrt{L_g C_g}$ the ideal frequency can be obtained by changing the cavity inductance. This is accomplished by changing the bias field within the ferrites and is refered to as tuning the cavity. Dynamic tuning refers to continuously changing the ferrite bias so that equation (12) is satisfied throughout the cycle. For SNS with 2×10^{14} protons and $\hat{V}_g = 6.7$ kV, the inductance per gap needs to drop from 7.5μH to 5.7μH during 1ms. The RF magnetic field will be $\sim$ 300G so the ferrites are changing quickly under high field conditions. Experiments are needed to test this scenario.

Experiments have been done on a parallel LRC circuit. The inductance was provided by two ferrite cores with 4 RF coupling turns, and the cores were in parallel. A 1 kΩ resistor, and a 2.9 nF of capacitor completed the circuit. For no tuning current the measured inductance of the ferrites measured in parallel $L = 9.8\mu$H. This gives a bare resonant frequency of 944 kHz. The drive frequency was swept from 1.092 MHz to 1.249 MHz over 1 ms and the system was pulsed at 60 Hz.

With a constant bias current, and a nearly constant drive current amplitude, the RF voltage dropped from 390 V to 65 V during the frequency sweep. When the bias current

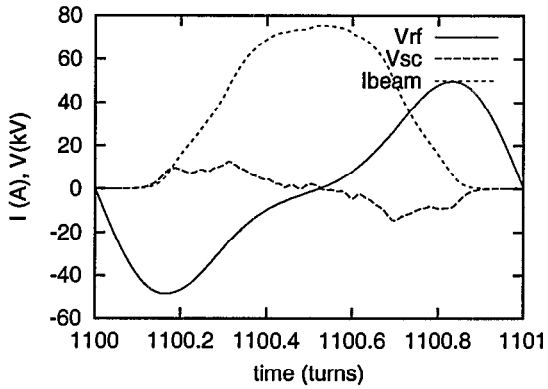

Figure 5: Currents and voltages at extraction for no feed forward.The binned current, convolved with a 50ns smoothing pulse, is shown.

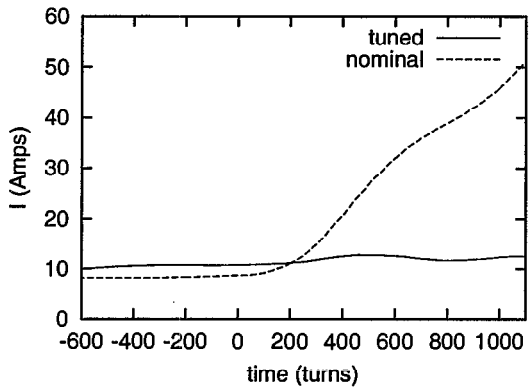

Figure 7: DC anode current during the cycle for the nominal case and with dynamic tuning.

was ramped linearly during the sweep, with the same drive current amplitude, the RF voltage remained nearly constant at 275 V. Optimal results required the bias current to be reversed between RF pulses to reset the ferrite hysteresis curve. The reduction in peak voltage is due to dynamic loss within the ferrite and can be compensated by increasing the drive.

With four coupling turns and 300 V, these experiments test an equivalent gap voltage of 1.6 kV. Further tests are needed to check operating conditions. Under the assumption that the ferrite tests will succeed, simulations have included dynamic tuning. Figures 6 and 7 show its clear benefits.

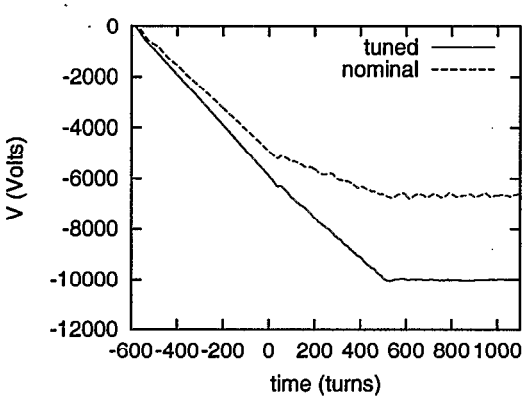

Figure 6: In phase amplitude of gap voltage (I_g) during the cycle for the nominal case and with dynamic tuning.

In both cases, the RF drive starts turning on 600 turns before injection starts (turn 0). For the nominal case the inductance is held constant at 7.5 μH while for the tuned case the inductance varies linearly with time. At turn 0 the tuned inductance is $L_g = 7.5$ μH while at turn 1100 (extraction) it is $L_g = 6.2$ μH. The $h = 1$ gap voltage in the tuned case corresponds to 60 kV/turn as compared with the nominal 40 kV/turn. The $h = 2$ voltage ramped from 15kV to 20 kV in both cases. The average anode current is significantly smaller for the tuned case. This is true even though the anode power supply voltage is $B^+ = 12$ kV for the tuned case and $B^+ = 10$ kV for the nominal case. Additionally, the total energy deposited in the anode each SNS cycle is significantly smaller for the tuned case.

5 ACKNOWLEDGEMENTS

Many people have contributed to this work. In particular we thank D. Boussard, Y.Y. Lee, D. Raparia, K. Rogers, R. Spitz, and R. Sanders.

6 REFERENCES

[1] National Spallation Neutron Source, Conceptual Design Report, 4-64, (1997).

[2] J. Wei, 7th European Particle Accelerator Conference,pg 123, (2000).

[3] M. Blaskiewicz, J.M. Brennan, Y.Y. Lee SNS tech note # 9, (1996).

[4] M. Blaskiewicz, J.M. Brennan, A. Zaltsman SNS tech note # 36, (1997).

[5] M. Blaskiewicz, J.M. Brennan, J. Brodowski, J. Delong, M. Meth, E. Onillon, A. Zaltsman , 7th European Particle Accelerator Conference,pg 1942, (2000).

[6] F. Pederson, IEEE, TNS, Vol. NS-22, No. 3, pg 1906, (1975).

[7] R. Garoby, Fontiers of Particle Beams: Intensity Limitations, US-CERN School on Particle Accelerators, Springer-Verlag, pg 509, (1990).

[8] D. Boussard, CERN 91-04 (1991).

[9] S. Koscielniak, TRI-DN-97 (1997) *and references therein*

[10] S.Y. Zhang, SNS Tech Note # 43 (1999).